



Microwave-assisted synthesis, characterizations, antimicrobial activities, and DFT studies on some pyridine derived Schiff bases

M. Ayaz^{a,b}, Ö. Gündoğdu^c, S. Aytaç^c, B. Erdem^d, H. Çiftçi^e, Y. Erdogdu^{a,*}

^a Graduate School of Natural and Applied Sciences, Department of Physics, Gazi University, Teknikokullar, Ankara 06400, Turkey

^b Science Faculty, Department of Physics, Gazi University, Teknikokullar, Ankara 06400, Turkey

^c Kaman Technical and Vocational School, Department of Food Technology, Kırşehir Ahi Evran University, Kırşehir 40300, Turkey

^d Vocational School of Health Services, Department of Medical Services and Techniques, Kırşehir Ahi Evran University, Kırşehir 40100, Turkey

^e Faculty of Medicine, Department of Medical Biochemistry, Kırşehir Ahi Evran University, Kırşehir 40100, Turkey

ARTICLE INFO

Article history:

Received 11 March 2022

Revised 21 July 2022

Accepted 22 July 2022

Available online 24 July 2022

Keywords:

Schiff bases

Microwave synthesis

Characterizations

Antimicrobial activities

DFT

ABSTRACT

This study reports a joint experimental, theoretical and microbiological investigation on the (*E*)-*N,N*-dimethyl-4-((pyridine-2-ylmethylene)amino)aniline (**5**), (*E*)-*N,N*-dimethyl-4-((pyridine-4-ylmethylene)amino)aniline (**6**) and (*E*)-*N,N*-dimethyl-4-((pyridine-3-ylmethylene)amino)aniline (**7**). These compounds were synthesized with microwave method and their structures characterized by FT-IR, ¹H-NMR, ¹³C-NMR, and elemental analysis techniques. In the theoretical studies, torsional barriers analysis, ground state structure, Fourier Transform Infrared spectra (FT-IR), and Nuclear Magnetic Resonance spectra (NMR) of **5**, **6**, and **7** were calculated by Density Functional Theory (DFT) computations. The conformers obtained from the torsional barrier scanning were optimized by B3LYP/6-31G(d,p) level. The harmonic vibrational frequencies, potential energy distribution (PED), infrared intensities, and NMR chemical shifts of the most stable conformers were determined using the B3LYP/6-311++G(d,p). Theoretically, predicted spectral data were compared with experimental results. Antimicrobial studies of the synthesized compounds were performed against various microbial strains. Antimicrobial activities of **5**, **6**, and **7** were tested against selected bacteria and yeast through minimum inhibitory concentration (MIC) and diffusion method. Compound **7** was found to be the most active against bacteria and yeast, while compound **5** was found to be moderately active. Compounds **6** (against *S. aureus* and *C. albicans*) and **7** were found to have a very high minimum inhibitory concentration, ranging between 1.95 and 7.81 g/mL (against *P. aeruginosa* and *E. coli*). Compounds (**6** and **7**) showed zone of inhibition values in the range of 10–20 mm against other bacteria except *L. monocytogenes* and *S. typhimurium*.

© 2022 Elsevier B.V. All rights reserved.

1. Introduction

Heterocycles are important organic structures, and they are commonly found in many synthetic drug molecules. Over 70% of pharmaceutical products contain heterocyclic substructures, which demonstrates their importance in therapeutic research and discovery [1]. Large amounts of pyridine are used as an intermediate agent in the synthesis of substituted pyridines, piperidine, agrochemicals (herbicides, fungicides, etc.) pharmaceuticals, and other products [2]. Pharmacophores containing pyridine make up an essential part of the pharmaceutical industry.

Pyridine is a crucial aromatic heterocyclic organic solvent and reagent [3]. The primary source of the pyridine molecule is coal tar, but the amount of pyridine is very low [4]. In 1876, Ram-

sey discovered the original laboratory synthesis of pyridine from the reaction of acetylene and hydrogen cyanide [5,6]. Water and organic solvents dissolve quickly with it. This property is used in the synthesis of drugs, nicotine, niacin, vitamins, food flavors, dyes, insecticides, rubber products, adhesives, and waterproof fabrics. Pyridine is also employed as a precursor for various agrochemicals and pharmaceuticals due to its chemical properties. As a result, pyridine and its derivatives have a wide range of applications, particularly in medicine [7,8]. Six-membered aromatic pyridines containing nitrogen and their derivatives are abundant, and they play an important role in heterocyclic chemistry [9]. Pyridine is used as a pharmacophore for agrochemicals [3]. Antiviral, anti-HIV, anticancer, antitumor, antibacterial, antimalarial, anti-inflammatory, antidiabetic, and antioxidant properties are among the several medicinal properties of pyridine derivatives [9–11].

Schiff bases with pyridine nucleus have critical biological activities. Pyridine Schiff bases are argued to be biologically impor-

* Corresponding author.

E-mail address: yerdogdu@gazi.edu.tr (Y. Erdogdu).

tant due to the similarity of the pyridine nucleus in many natural products such as some vitamins and enzymes [12]. Several methods for the synthesis of Schiff bases have been reported. However, many of them have disadvantages such as lower yields, harsh reaction conditions, prolonged reaction times, and the use of excessive amounts of catalysts. For this reason, new, effective, and economical synthesis methods are needed for the synthesis of Schiff compounds [13]. They are traditionally prepared by refluxing mixtures of the amine and the carbonyl compound in a solvent such as ethanol [14], methanol [14], tetrahydrofuran (THF) and, 1, 2-dichloroethane [15] and acids are used as a catalyst and then water is released in the reaction [16]. In addition to classical heating methods, many new techniques and innovations have been reported to synthesize Schiff bases in the past two decades. This technique includes solvent-free/clay/microwave irradiation, K-10/microwave, infrared irradiation/no solvent, water suspension medium, $\text{NaHSO}_4/\text{SiO}_2$ /microwave/solvent-free, solid-state synthesis, and silica/ultrasound irradiation [17]. The microwave power technique that is frequently used in organic synthesis [18]. This technique shortens the reaction time, reduces by-product formation and evaporation of solvents, and provides a high yield product [19].

In this study, the synthesis of pyridine derivative Schiff Bases and their theoretical and microbiological investigation were aimed. Compound **5** and **6** synthesized for the first time by our group using microwave method because it is a cheap, quick, and ecologically friendly process [20]. Compound **7** has been documented in the literature [21]. We also used the microwave to re-synthesize compound **7**. Structures of the all compounds were characterized by elemental analysis, ^1H NMR, ^{13}C NMR, and FT-IR spectroscopy. This study further provides the theoretical results of a systematic study of torsional barrier analysis, vibrational spectra, and NMR spectra of **5**, **6**, and **7** by DFT computations. Examining the antimicrobial properties of compounds **5**, **6** and **7** is another aim of the study. The antimicrobial activities of **5**, **6** and **7** were investigated against selected bacteria and yeasts using the agar well diffusion and microdilution broth method.

2. Materials and methods

2.1. Chemical material and apparatus

All chemicals were purchased commercially from Merck and Sigma-Aldrich. Solvents were of analytical grade and were obtained from Sigma-Aldrich, and they were used without further purification. The reactions were monitored by thin-layer chromatography (TLC). ^1H NMR and ^{13}C NMR spectra were recorded with Varian spectrometer at 400 and 100 MHz using CDCl_3 as reference. Melting points were determined in a capillary melting apparatus (BUCHI 530). The reactions were carried out with a Vestel MD 20 DB model microwave oven (230 V-50 Hz, 900 W). The IR spectrum was recorded with a Perkin Elmer spectrophotometer using an ATR head in the range of $4000\text{--}600\text{ cm}^{-1}$. Elemental analysis was performed on a Leco CHNS-932 instrument.

2.2. General synthesis of Schiff bases

N,N-dimethylbenzene-1,4-diamine (**1**) (1 mmol) was placed in a balloon. Aryl aldehyde compounds (isonicotinaldehyde (**2**), nicotinaldehyde (**3**), and picolinaldehyde (**4**)) were added separately as 1 mmol. The reaction mixture was exposed to microwave radiation at 900 W in solvent-free conditions (Fig. 1) [22]. The progress of the reaction was monitored by TLC. It was determined that the reactions were completed in 5 min for all aromatic derivatives. The resulting compounds were purified by crystallization in DCM/P.Ether or Methanol/P.Ether. When the ^1H NMR and ^{13}C NMR

spectra of the residue were examined, it was determined that the compounds (**5**, **6**, and **7**) formed as single compounds.

2.3. Computational details

DFT calculations were made using Gaussian 16 software [23]. DFT/B3LYP functional were used in all calculations [24–26]. 6-31G(d,p) and 6-311++G(d,p) basis sets were used with B3LYP functional. While the 6-31G(d,p) basis set were used in the optimization of the conformers, the 6-311++G(d,p) basis set were used in all other calculations.

The theoretical NMR data of **5**, **6**, and **7** were predicted by Gauge Independent Atomic Orbital (GIAO) method. These calculations were done in chloroform solution using IEF-PCM model. The predicted ^1H and ^{13}C NMR data were matched with experimental ones. Identification and characterization of the compounds could be done in more detail by this matching. Absolute isotropic magnetic shielding constants were converted into chemical shifts. This conversion was performed relative to tetramethylsilane (TMS), the compound used as a standard [27,28].

The stable conformers of the molecular system were determined before starting calculations of other molecular properties of examined system. For these calculations, the torsional barrier analysis was calculated first. Torsional barrier analysis was performed by examining conformational distribution using Gaussian 16 software [29]. In the torsional barrier analysis, B3LYP/6-31G(d,p) level of theory [30] was used to identify all possible conformers.

2.4. Antimicrobial activity of the compounds

In the present study, Agar Well Diffusion Method and Microdilution Broth Method were used to determine the *in vitro* antimicrobial effects of newly synthesized compounds. Each standard strain of fresh cultures was harvested, and the prepared suspension was inoculated into each other well to reach a final concentration of 5×10^6 CFU/ml.

Inoculated test bacteria were placed in Nutrient Broth (Difco) and incubated for 24–48 h. Mueller Hinton Agar (Oxoid) was used in the agar well diffusion method to count bacteria and yeast (10^6 per mL) for 24 to 48 h. The culture plate wells were drilled with a sterile cork borer (7 mm diameter). A stock solution of newly synthesized compounds (1.0 mg/mL) in ethyl acetate was prepared and mixed in a petri dish opening (Mueller Hinton Agar for bacteria and Sabouraud dextrose agar medium for yeasts) (3 mm depth, 4 mm diameter). Following the addition of the compounds, the plates were incubated in duplicate for 48 h at 37 °C (for bacteria) and 30 °C (for yeast). The inhibition zones formed on the agar plates were later measured in millimeters (mm). Positive controls included ampicillin and cycloheximide. Each step of the disk diffusion method was carried out by the NCCLS guidelines [31]. The results of antimicrobial screening of synthesized and standard antibiotics were shown in Table 8.

Minimum inhibitory concentrations (MIC) for compounds against bacteria and yeast strains were examined by the NCCLS guideline [31]. Mueller-Hinton broth was used in the suspension of bacteria (0.5 McFarland), in solutions of substances to be tested (1000 $\mu\text{g/mL}$ in ethyl acetate), and in MIC testing. MIC values were determined spectrophotometrically in 96-well microtiter plates based on the microdilution broth method. Ten standard fresh strain cultures were used for MIC measurements. In 96-well plates containing 100 μL of 250, 125, 62.5, 31.2, and 15.6 $\mu\text{g/mL}$ of compounds, 100 μL of inoculum were seeded in duplicate and were allowed to grow overnight with the flow at 37 °C. To determine MIC by Microdilution Broth method; 96-well sterile 100 μL of NB medium was added to all wells of the microtiter plates with an automatic dispenser device (BioTek, Micro Fill). The absorbance

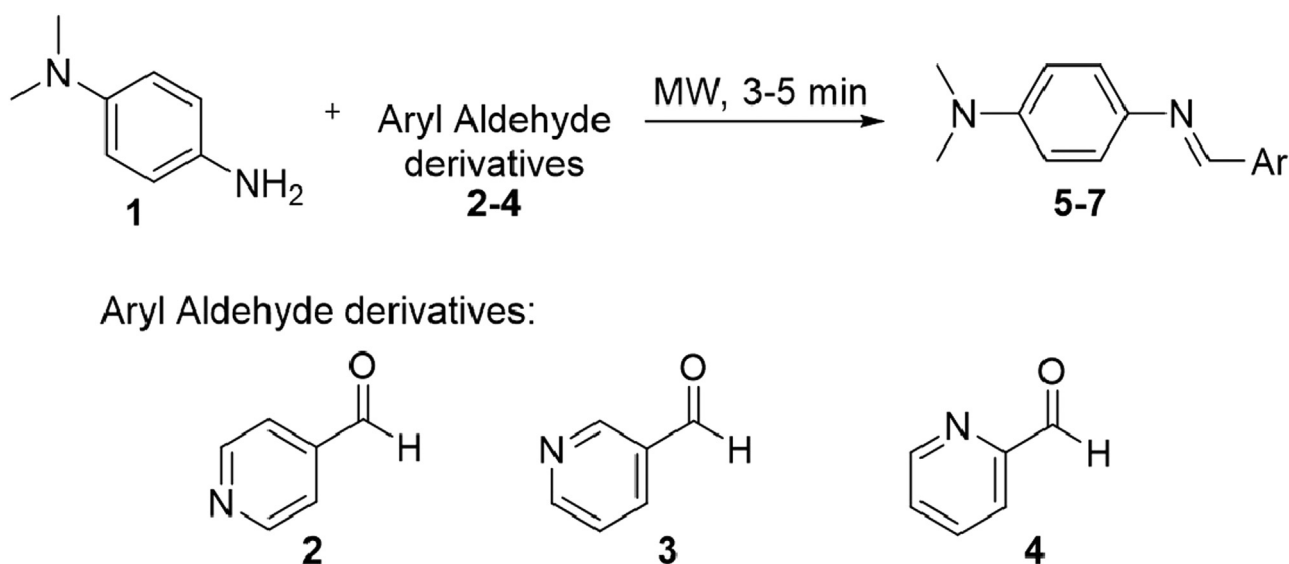


Fig. 1. General procedure for the synthesis of Schiff base compounds.

at 590 nm wavelength was measured with a microplate reader (BioTek, μ Quant) of plates incubated at 37 °C for 24 h. The nutrient broth was used as a negative control. The positive control contained the microorganisms.

3. Results and discussion

3.1. Chemistry

A series of Pyridine-Based Schiff Bases were prepared by reacting various aldehyde in the presence of microwave irradiation which is a cheap, fast and more environmentally friendly method [22]. These compounds (**5-7**) were synthesized in 96%, 95% and 94% yields, respectively. In this procedure, the solvent-free reaction of *N,N*-dimethylbenzene-1,4-diamine (**1**) and Aryl aldehyde (isonicotinaldehyde (**2**), nicotinaldehyde (**3**), and picotinaldehyde (**4**)) compounds by exposing to microwave radiation at 900 W without solvent.

The structures of synthesized compounds characterized by IR, ^1H NMR, ^{13}C NMR, Elemental Analysis and other physical data. The formation of Schiff bases (**5-7**) was confirmed by IR and NMR spectra. The bands at 1619, 1621, 1574 cm^{-1} are due to the characteristic carbonyl C=N (imine bond) stretching. The proton in the H-C=N bond causes the peaks in the ^1H NMR spectra at 8.52, 8.57, and 8.21 ppm. In addition, the peaks in the ^{13}C NMR spectra at 152.1, 151.9, and 155.4 ppm indicate the carbon atom in the H-C=N bond in the compounds.

3.2. Spectral data and physical properties of the synthesized compounds

(*E*)-*N,N*-dimethyl-4-((pyridin-4-ylmethylene)amino)aniline (**5**):

Yield 96%, green solid, m.p: 195–196 °C, R_f : 0.2 (Ethyl acetate/Petroleum ether, 1:1), (Lit:191–192 °C [32]). ^1H NMR (400 MHz, CDCl_3) δ 8.73 (dd, $J = 4.5, 1.5$ Hz, 2H, H_1 and H_1'), 8.52 (s, 1H, N=CH, H_3), 7.75 (dd, $J = 4.5, 1.6$ Hz, 2H, H_2 and H_2'), 7.40–7.32 (m, 2H, H_4 and H_4'), 6.82–6.74 (m, 2H, H_5 and H_5'), 3.05 (s, 6H, $\text{N}(\text{CH}_3)_2$) ppm. ^{13}C NMR (100 MHz, CDCl_3) δ 152.1, 150.3 (2C), 143.7, 139.2, 122.8, 121.8, 112.5, 40.5 ppm. FT-IR (cm^{-1}): 1619 (C=N), 1582 (C=C aromatic), 1408, 1361(C-N), 1232. Elemental Anal. Calcd. for $\text{C}_{14}\text{H}_{15}\text{N}_3$ C, 74.64; H, 6.71; N, 18.65 Found: C, 74.72; H, 6.70; N, 18.60.

(*E*)-*N,N*-dimethyl-4-((pyridin-3-ylmethylene)amino)aniline (**6**):

Yield: 95%, green solid, m.p: 112–113 °C, R_f : 0.3 (Ethyl acetate/Petroleum ether, 3:7) ^1H NMR (400 MHz, CDCl_3) δ 9.00 (d, $J = 1.8$ Hz, 1H, H_3), 8.66 (dd, $J = 4.8, 1.6$ Hz, 1H, H_2), 8.57 (s, 1H, N=CH, H_5), 8.29 (dt, $J = 8.0, 1.9$ Hz, 1H, H_4), 7.39 (dd, $J = 7.9, 4.8$ Hz, 1H, H_1), 7.32 (d, $J = 9.0$ Hz, 2H, H_6 and H_6'), 6.78 (d, $J = 9.0$ Hz, 2H, H_7' and H_7), 3.02 (s, 6H, $2\times\text{CH}_3$) ppm. ^{13}C NMR (100 MHz, CDCl_3) δ 151.9, 151.1, 150.5, 149.9, 140.0, 134.3, 132.5, 123.7, 122.4, 112.7, 40.6 ppm. FT-IR (cm^{-1}): 1621(C=N), 1517(C=C aromatic), 1421, 1358 (C-N), 1231. Elemental Anal. Calcd. for $\text{C}_{14}\text{H}_{15}\text{N}_3$ C, 74.64; H, 6.71; N, 18.65 Found: C, 74.62; H, 6.71; N, 18.74

(*E*)-*N,N*-dimethyl-4-((pyridin-2-ylmethylene)amino)aniline (**7**):

94% yield, green solid, m.p: 90–92 °C, R_f : 0.36 (Ethyl acetate/Petroleum ether, 3:7) ^1H NMR (400 MHz, CDCl_3) δ 8.70 (d, $J = 5.0$ Hz, 2H, H_3 and H_4), 8.21 (d, $J = 8.0$ Hz, 1H, N=CH, H_5), 7.79 (td, $J = 7.7, 1.7$ Hz, 1H, H_1), 7.42–7.37 (m, 2H, H_6 and H_6'), 7.32 (ddd, $J = 7.5, 4.8, 1.2$ Hz, 1H, H_2), 6.81–6.76 (m, 2H, H_7 and H_7'), 3.03 (s, 6H, $2\times\text{CH}_3$) ppm. ^{13}C NMR (100 MHz, CDCl_3) δ 155.4, 155.3, 150.1, 149.5, 139.4, 136.4, 124.2, 122.9, 121.3, 112.6, 40.5 ppm. FT-IR (cm^{-1}): 1574 (C=N), 1516 (C=C aromatic), 1358 (C-N), 1166. Elemental Anal. Calcd. for $\text{C}_{14}\text{H}_{15}\text{N}_3$ C, 74.64; H, 6.71; N, 18.65 Found: C, 74.58; H, 6.78; N, 18.58.

3.3. Torsional barrier analysis and molecular structure

Atomic numbering and molecular structures of **5**, **6**, and **7** was given in Fig. 2. The torsional analysis of **5**, **6**, and **7** was run by considering the bonds shown by the **1**, **2**, and **3** in Fig. 2. The dihedral angles of the PES scan were carried out around the bond CH-Pyridine group (**I**), N=CH (**II**), and C-N(CH_3)₂ (**III**) by changing the dihedral angle at 10 steps from 0 to 360. According to the PES scan result (Fig. S5), two conformers of the **5**, two conformers of the **6**, and four conformers of the **7** were determined using the B3LYP/6-31G(d,p) level of theory in the Gaussian 16 program in Table 1.

The optimized geometric structure, optimized energies, relative energies, Dipole moment, Boltzmann population distribution and dihedral angles of conformers were provided in Table 1. According to these results, the relative energies conformer-1 and conformer-2 of **5** were predicted at 0.00 kcal/mol, 0.0538 kcal/mol, respectively. Them of conformer-1 and conformer-2 of **6** determined at 0.00 kcal/mol, 0.0580 kcal/mol, respectively. Compound **7** has four

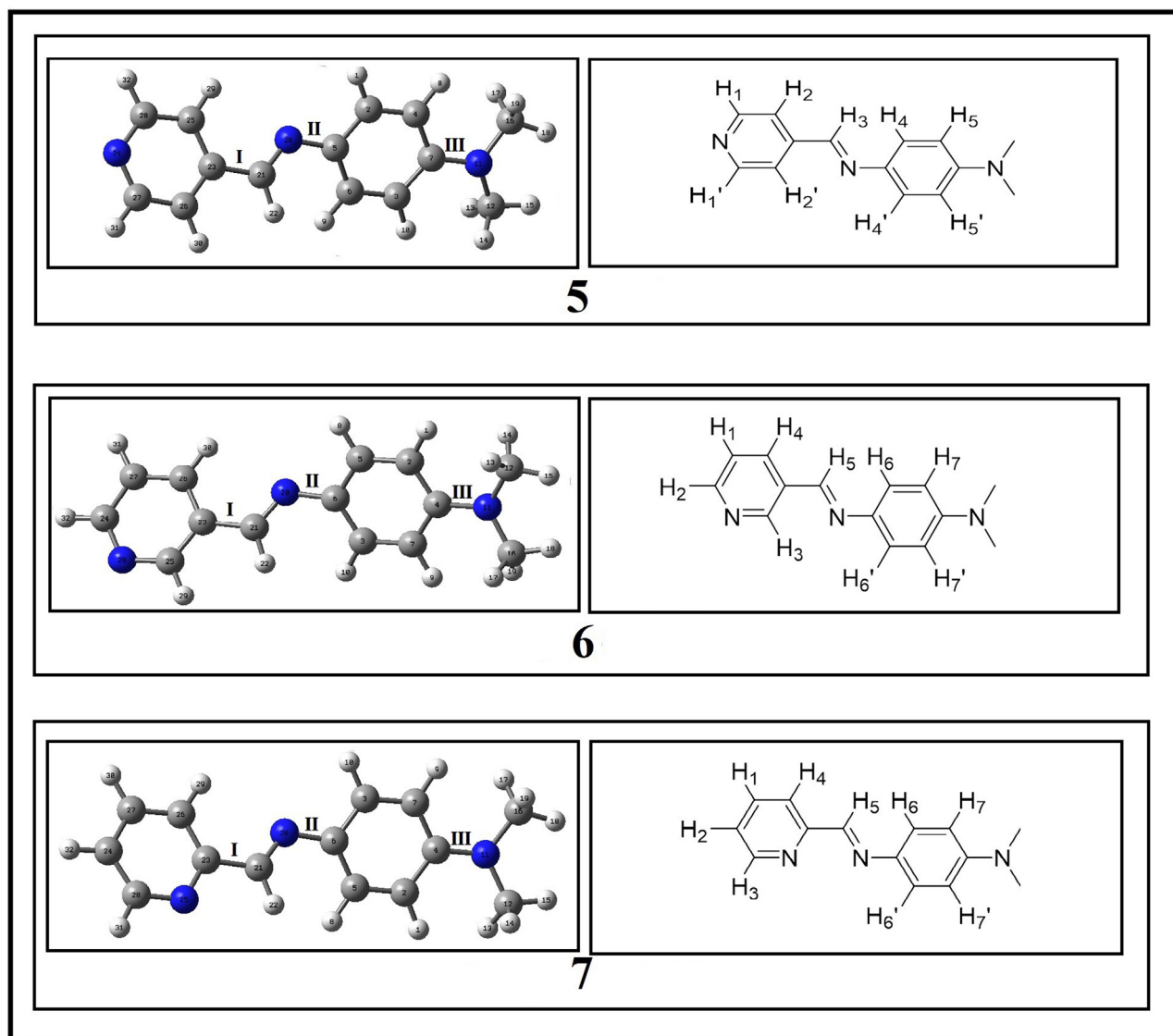


Fig. 2. Atomic numbering and molecular structures of **5**, **6** and, **7**.

conformers with relative energies 0.00 kcal/mol, 0.0480 kcal/mol, 4.911 kcal/mol and 4.983 kcal/mol. The parameters such as optimized energies, relative energies, dipol moment, population and dihedral angles of the conformer 1 and 2 of compounds were determined to be very close to each other. Compared to conformers of **7**, conformer 3 and 4 have higher energies. We made all future calculations with conformer 1 of the compounds. The optimized molecular parameters obtained as a result of the calculations of the conformer-1 of all compounds were presented in Table S1 as supplementary material.

3.4. Vibrational assignment

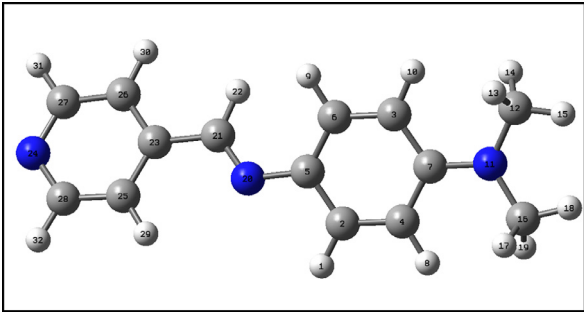
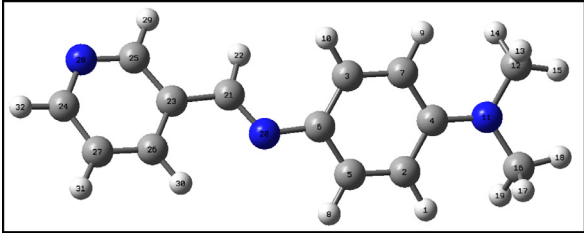
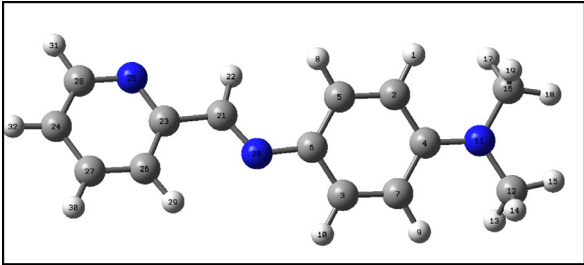
5, **6**, and, **7** have 32 atoms, and thus it has 90 normal modes. **5**, **6**, and, **7** have the C_1 symmetry. All fundamental vibrations are active in the infrared spectra. The measured and calculated frequencies were tabulated in Tables 2–4. We scaled the computed frequencies in the harmonic approximation to closely reproduce the experimental value. A scaling factor of 0.988 was used for wavenumbers below 1800, and a scaling factor of 0.960 was used for wavenumbers above 1800 [33]. The experimental FT-IR of **5**, **6**, and, **7** was shown in Fig. S1. Comparing the observed and calcu-

lated spectral data of compounds **5**, **6**, and, **7**, it was possible to notice that both spectral data overlapped well.

The characteristic band of H–C=N stretching vibration in the imine group was observed at a medium peak in the 1690–1640 cm^{-1} range. This peak predicted as 1658 cm^{-1} for **5**, 1658 cm^{-1} for **6**, and 1659 cm^{-1} for **7** by DFT calculation. The observed 1619 cm^{-1} peak was assigned as imine group vibrations of **5**. Similarly, 1621 and 1619 were detected for **6** and, **7**. PED contributions of these peaks were determined as 40–45% for CC, CN stretching and 30–35% for CCC and CCH bending vibrations.

Observed wave numbers between 3092 and 2814 cm^{-1} were determined as CH stretching of the phenyl group (3092 cm^{-1}), CH stretching of the pyridine group (3071 and 3031 cm^{-1}), CH stretching of the H–C=N (imine group, 2888 cm^{-1}), and CH_3 stretching of the methyl group (2814 cm^{-1}) in the FT-IR spectra of the **5**, respectively. In the FT-IR spectra of **6**, 3036, 2886 and 2810 cm^{-1} as assigned to the CH stretching of the pyridine group, the H–C=N (imine group) and the CH_3 stretching of the methyl group, respectively. The CH stretching vibration of the phenyl group, the methyl group, imine group, and the CH_3 stretching of the methyl group of **7** were measured at 3046, 3008, 2924 and 2080 cm^{-1} in the FT-IR spectra, respectively. The CH vibrations of the pyridine group of **7**

Table 1
Torsional Barrier results of **5**, **6**, and **7** compounds.

Compound-5				
				
	Conformer-1		Conformer-2	
Optimized Energy (a.u.)	-706.77712108		-706.77703529	
Relative Energy (kcal/mol)	0.000		0.0538	
Dipol Moment (Debye)	6.142		6.251	
Population (298 K)/%	52.26		47.73	
C ₂₁ -N ₂₀ -C ₅ -C ₆ Dihedral Angel	24.52		23.55	
C ₃ -C ₇ -N ₁₁ -C ₁₂ Dihedral Angel	7.48		-175.19	
N ₂₀ -C ₂₁ -C ₂₃ -C ₂₅ Dihedral Angel	0.64		0.72	
Compound-6				
				
	Conformer-1		Conformer-2	
Optimized Energy (a.u.)	-706.77763686		-706.77754454	
Relative Energy (kcal/mol)	0.000		0.0580	
Dipol Moment (Debye)	4.408		4.960	
Population (298 K)/%	52.44		47.55	
C ₂₁ -N ₂₀ -C ₆ -C ₃ Dihedral Angel	25.74		S2	26.51
C ₇ -C ₄ -N ₁₁ -C ₁₆ Dihedral Angel	-9.87		S3	169.46
N ₂₀ -C ₂₁ -C ₂₃ -C ₂₆ Dihedral Angel	1.02		S1	-179.00
Compound-7				
				
	Conformer-1	Conformer-2	Conformer-3	Conformer-4
Optimized Energy (a.u.)	-706.77959086	-706.77951349	-706.77176386	-706.77164931
Relative Energy (kcal/mol)	0.000	0.048	4.911	4.983
Dipol Moment (Debye)	2.541	2.516	3.200	3.417
Population (298 K)/%	50.70	49.27	0.01	0.01
C ₅ -C ₆ -N ₂₀ -C ₂₁ Dihedral Angel	23.82	22.83	27.71	26.82
C ₇ -C ₄ -N ₁₁ -C ₁₆ Dihedral Angel	-171.22	8.13	10.64	8.27
N ₂₀ -C ₂₁ -C ₂₃ -C ₂₆ Dihedral Angel	0.24	0.36	-170.73	-178.39

Torsional barrier calculations were performed by B3LYP/6-31G(d,p) level of theory.

could not be observed in the FT-IR spectra. In addition, CH vibrations of the CH₃ group of **5** and **6** could not be observed. Besides, from the vibrations, it could be seen that there was a perfect similarity.

3.5. NMR spectra

The theoretical ¹H and ¹³C NMR chemical shifts of the **5**, **6**, and **7** were predicted through the GIAO method. The researchers com-

Table 2
Experimental and predicted vibrational wavenumber for **5** at B3LYP/6-311++G(d,p).

FT-IR	Freq ^a	Freq ^b	I _{IR} ^c	TED ^d
515	517	519	3.523	$\tau_{\text{CCCH}}(20\%) + \tau_{\text{HCCN}}(15\%) + \tau_{\text{CCCC}}(10\%) + \tau_{\text{CNCC}}(11\%)$
548	552	551	7.366	$\tau_{\text{CCCH}}(32\%) + \tau_{\text{CCNC}}(30\%) + \tau_{\text{HCCN}}(16\%) + \tau_{\text{CCCC}}(15\%)$
617	621	621	2.461	$\delta_{\text{CCC}}(18\%) + \delta_{\text{CCH}}(15\%) + \delta_{\text{CCN}}(11\%) + \delta_{\text{CNC}}(10\%)$
739	733	731	0.402	$\tau_{\text{CCCH}}(21\%) + \tau_{\text{CCCC}}(19\%) + \tau_{\text{CNCC}}(13\%)$
814	816	816	1.023	$\tau_{\text{HCCN}}(43\%) + \tau_{\text{CCCH}}(41\%) + \tau_{\text{CCCC}}(10\%)$
826	828	827	15.95	$\tau_{\text{CCCH}}(38\%) + \tau_{\text{HCCN}}(30\%) + \tau_{\text{CCCC}}(11\%)$
884	887	886	1.099	$\nu_{\text{CC}}(13\%) + \delta_{\text{CCH}}(11\%) + \delta_{\text{CNC}}(10\%) + \tau_{\text{CCCH}}(10\%)$
936	935	935	0.798	$\tau_{\text{CCCH}}(50\%) + \tau_{\text{CNCH}}(20\%) + \tau_{\text{CCCC}}(14\%) + \tau_{\text{HCCN}}(11\%)$
947	949	950	6.718	$\tau_{\text{CCCH}}(29\%) + \tau_{\text{HCCN}}(15\%) + \nu_{\text{CN}}(11\%) + \delta_{\text{HCN}}(10\%)$
970	978	978	1.256	$\tau_{\text{CCCH}}(50\%) + \tau_{\text{HCCN}}(13\%)$
1067	1069	1069	0.325	$\delta_{\text{CCH}}(41\%) + \nu_{\text{CC}}(15\%) + \nu_{\text{CN}}(11\%) + \delta_{\text{CNC}}(10\%)$
1083	1092	1092	0.020	$\delta_{\text{CCH}}(48\%) + \nu_{\text{CC}}(17\%)$
1125	1127	1126	17.37	$\tau_{\text{HCCN}}(36\%) + \delta_{\text{HCH}}(27\%)$
1168	1172	1172	19.43	$\delta_{\text{CCH}}(25\%) + \tau_{\text{HCCN}}(17\%) + \nu_{\text{CC}}(12\%) + \delta_{\text{HCH}}(13\%)$
1212	1208	1208	1.163	$\delta_{\text{CCH}}(46\%) + \nu_{\text{CC}}(15\%) + \delta_{\text{CCC}}(13\%)$
1232	1244	1246	7.839	$\tau_{\text{HCCN}}(20\%) + \nu_{\text{CC}}(18\%) + \delta_{\text{CCH}}(16\%) + \nu_{\text{CN}}(13\%) + \delta_{\text{HCH}}(13\%)$
1321	1333	1333	0.392	$\delta_{\text{CCH}}(51\%) + \nu_{\text{CC}}(13\%) + \delta_{\text{HCH}}(13\%)$
1361	1360	1361	71.78	$\delta_{\text{HCCN}}(22\%) + \delta_{\text{CCH}}(17\%) + \delta_{\text{HCH}}(13\%) + \delta_{\text{HCH}}(13\%) + \nu_{\text{CN}}(12\%)$
1408	1424	1424	4.232	$\delta_{\text{CCH}}(38\%) + \delta_{\text{HCH}}(23\%) + \nu_{\text{CC}}(13\%)$
1444	1447	1448	0.676	$\delta_{\text{CCH}}(31\%) + \delta_{\text{HCH}}(13\%) + \delta_{\text{HCH}}(13\%) + \tau_{\text{HCCN}}(11\%)$
1459	1467	1468	7.156	$\delta_{\text{HCH}}(30\%) + \delta_{\text{HCH}}(29\%) + \delta_{\text{CCH}}(15\%) + \tau_{\text{HCCN}}(11\%)$
1518	1511	1511	8.787	$\tau_{\text{HCCN}}(31\%) + \delta_{\text{HCH}}(29\%) + \delta_{\text{CCH}}(17\%) + \delta_{\text{HCH}}(12\%)$
1542	1529	1529	42.25	$\delta_{\text{CCH}}(32\%) + \delta_{\text{HCH}}(24\%) + \nu_{\text{CC}}(13\%)$
1583	1598	1598	100	$\delta_{\text{CCH}}(33\%) + \nu_{\text{CC}}(25\%) + \delta_{\text{CCC}}(12\%)$
1619	1622	1622	6.707	$\delta_{\text{CCH}}(33\%) + \nu_{\text{CC}}(26\%) + \delta_{\text{CCC}}(12\%)$
2814	2858	2860	30.77	$\nu_{\text{CH}}(78\%)$
2888	2891	2891	9.822	$\nu_{\text{CH}}(78\%)$
3034	3024	3024	5.409	$\nu_{\text{CH}}(79\%)$
3071	3075	3075	0.765	$\nu_{\text{CH}}(77\%)$
3092	3083	3082	2.950	$\nu_{\text{CH}}(80\%)$

ν : Stretching, δ : Bending, τ : Torsion.

^a Obtained from the wave number calculated at B3LYP/6-311++G(d,p) using scaling factors 0.960 in the high wavenumbers region and 0.988 in the low wavenumbers region [34]. (Conformer-1).

^b Obtained from the wave number calculated at B3LYP/6-311++G(d,p) using scaling factors 0.960 in the high wavenumbers region and 0.988 in the low wavenumbers region [34]. (Conformer-2) Relative absorption intensities normalized with highest peak absorption equal to 100.

^d Total energy distribution calculated B3LYP/6-311++G(d,p) level, PED less than 10% are not shown.

pared the detected and predicted NMR data for ^1H and ^{13}C nuclei in Table 5. Experimental ^1H and ^{13}C NMR spectra of **5**, **6** and, **7** were given in Figs. S2–S4.

In the ^1H NMR spectra, the peak detected at 8.50 ppm for **5**, at 8.57 ppm for **6** and 8.70 ppm for **7** belonged to the proton in the H–C=N group. The chemical shift of H_{22} atoms was predicted at 8.70 ppm (**5**), 8.71 ppm (**6**), and 8.82 ppm (**7**) by DFT calculations. The C_{21} peaks of each compound were experimentally measured at 152.1 ppm (**5**), 150.5 ppm (**6**), and 155.4 ppm (**7**) in the ^{13}C NMR spectra. The C_{21} NMR chemical shift of each compound was calculated at 154.9 ppm (**5**), 154.2 ppm (**6**), and 159.2 ppm (**7**) by DFT calculations.

Peaks experimentally measured as 3.05 ppm (**5**), 3.02 ppm (**6**), and 3.03 ppm (**7**) belonged to the proton of the methyl groups. Predicted ^1H NMR chemical shift of each compound appeared at 3.39–2.76 ppm region by DFT. The ^{13}C NMR peaks were detected at 40.05 ppm (**5**), 40.06 ppm (**6**), and 40.05 ppm (**7**). The smallest ^{13}C NMR chemical shift values were theoretically calculated for the CH_3 group. Theoretical and experimental values for both ^1H and ^{13}C NMR seemed to be in good agreement. As expected, the theoretical and experimental ^{13}C NMR values, except for the methyl group, appeared above 100 ppm. The Carbon atoms attached to the Nitrogen atom with greater electronegativity were more de-shielded [34–37]. Therefore, these atoms had higher ^{13}C NMR peaks than other ones.

3.6. Frontier molecular orbital analysis (FMO)

The highest occupied molecular orbital (HOMO) and lowest unoccupied molecular orbital (LUMO) plots of the **5**, **6**, and, **7** were given in Fig. 3. The positive and negative phases were characterized in red and green colors, respectively. HOMO and LUMO were distributed over the entire compounds. However, this distribution was not homogeneous. It could be seen that LUMO was more concentrated in phenyl and N– CH_3 groups, while HOMO was more concentrated in the pyridine group. The HOMO, LUMO, bandgap energies, and other molecular parameters were determined at B3LYP/6-311++G(d,p) theory. Molecular parameters such as ionization potential (I), electron affinity (A), Mulliken's absolute electronegativity (χ), chemical potential (μ), spherical hardness (η), spherical softness (σ), and spherical electrophilicity (ω) were determined through the equations given in the footnote of Table 6 [38–40]. These properties were tabulated in Table 6.

It is clear from the literature that less reactivity and greater stability of any compound are associated with a larger HOMO-LUMO gap. The value of the HOMO-LUMO gap calculated for **5**, **6**, and, **7** was determined as 3.312 eV, 3.362 eV, and 3.381 eV, respectively. The smaller HOMO-LUMO gap is considered high reactivity. According to the calculation result, the reactivity of the compound **5** could be noted as being greater than the others. The HOMO and LUMO plot of **5**, **6**, and, **7** were illustrated in Fig. 3. The HOMO is

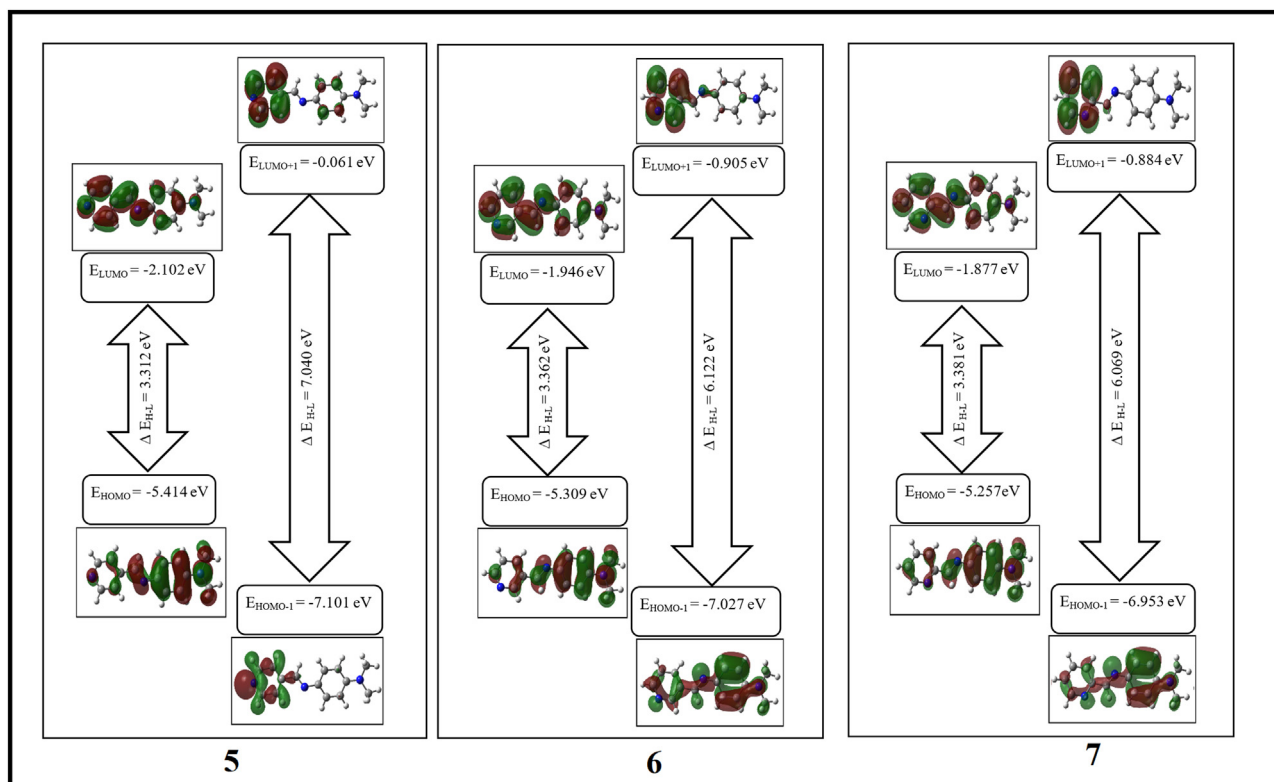


Fig. 3. HOMO and LUMO polts of **5**, **6** and **7**.

Table 3
Experimental and predicted vibrational wavenumber for **6** at B3LYP/6-311++G(d,p).

FT-IR	Freq ^a	Freq ^b	I _{IR} ^c	TED ^d
515	518	519	1.669	$\tau_{\text{CCH}}(22)+\tau_{\text{CNC}}(20)+\delta_{\text{CCC}}(10)$
545	544	545	5.697	$\tau_{\text{CCH}}(32)+\tau_{\text{CNC}}(17)+\tau_{\text{HCCN}}(14)+\tau_{\text{CCCC}}(12)$
614	617	617	0.680	$\delta_{\text{CCH}}(36)+\delta_{\text{CCC}}(20)+\delta_{\text{CCN}}(12)$
640	646	647	0.501	$\delta_{\text{CCH}}(27)+\delta_{\text{CCC}}(27)+\delta_{\text{CNC}}(11)$
702	711	711	9.090	$\tau_{\text{CCH}}(34)+\tau_{\text{CNC}}(31)+\tau_{\text{CCCC}}(17)$
720	725	723	0.617	$\tau_{\text{CCH}}(28)+\tau_{\text{CCCC}}(24)+\tau_{\text{CNC}}(15)$
813	809	809	1.783	$\tau_{\text{CCH}}(41)+\tau_{\text{HCCN}}(16)+\tau_{\text{CNC}}(10)$
824	823	823	22.30	$\tau_{\text{CCH}}(33)+\tau_{\text{HCH}}(22)+\tau_{\text{CNC}}(21)+\tau_{\text{CCCC}}(11)$
879	883	884	3.057	$\tau_{\text{CCH}}(15)+\nu_{\text{CC}}(14)+\delta_{\text{CCH}}(11)+\delta_{\text{CNC}}(10)$
935	934	934	0.833	$\tau_{\text{CCH}}(50)+\tau_{\text{HCCN}}(18)+\tau_{\text{CCCC}}(12)$
970	979	979	1.854	$\tau_{\text{CCH}}(39)+\tau_{\text{HCCN}}(19)+\tau_{\text{CNC}}(10)$
1021	1025	1025	2.943	$\delta_{\text{CCH}}(26)+\delta_{\text{CCC}}(25)+\nu_{\text{CC}}(14)+\delta_{\text{CNC}}(13)$
1066	1065	1065	7.141	$\tau_{\text{HCCN}}(37)+\delta_{\text{HCCN}}(31)+\delta_{\text{HCH}}(10)+\nu_{\text{CN}}(10)$
1124	1127	1128	21.77	$\tau_{\text{HCCN}}(35)+\delta_{\text{HCCN}}(27)$
1169	1173	1173	24.07	$\delta_{\text{CCH}}(25)+\tau_{\text{HCCN}}(18)+\delta_{\text{HCCN}}(15)+\nu_{\text{CC}}(13)$
1232	1244	1243	12.24	$\tau_{\text{HCCN}}(21)+\nu_{\text{CC}}(17)+\delta_{\text{CCH}}(16)+\delta_{\text{HCCN}}(13)$
1323	1337	1336	0.762	$\delta_{\text{CCH}}(49)+\delta_{\text{HCCN}}(13)+\nu_{\text{CC}}(10)$
1358	1358	1358	100	$\tau_{\text{HCCN}}(22)+\delta_{\text{CCH}}(17)+\delta_{\text{HCCN}}(13)+\delta_{\text{HCH}}(13)$
1422	1428	1428	1.048	$\delta_{\text{HCCN}}(26)+\delta_{\text{HCH}}(24)+\delta_{\text{CCH}}(16)+\tau_{\text{HCCN}}(10)$
1444	1447	1446	0.928	$\delta_{\text{CCH}}(30)+\delta_{\text{HCCN}}(14)+\delta_{\text{HCH}}(12)+\tau_{\text{HCCN}}(10)$
1518	1511	1510	10.70	$\tau_{\text{HCCN}}(33)+\delta_{\text{HCH}}(30)+\tau_{\text{CCH}}(14)+\delta_{\text{HCCN}}(10)$
1567	1567	1567	2.689	$\delta_{\text{CCH}}(27)+\nu_{\text{CC}}(25)+\delta_{\text{CCC}}(11)+\delta_{\text{CNC}}(11)$
1595	1600	1600	19.50	$\beta_{\text{CCH}}(32\%)+\nu_{\text{CC}}(22\%)+\beta_{\text{CCC}}(10\%)+\nu_{\text{CN}}(10\%)$
1621	1620	1620	66.83	$\delta_{\text{CCH}}(34)+\nu_{\text{CC}}(24)+\nu_{\text{CN}}(10)+\delta_{\text{CCC}}(13)$
2810	2856	2854	42.43	$\nu_{\text{CH}}(78)$
2886	2889	2889	13.80	$\nu_{\text{CH}}(78)$
3036	3024	3024	2.987	$\nu_{\text{CH}}(80)$

v: Stretching, δ : Bending, τ : Torsion.

^a Obtained from the wave number calculated at B3LYP/6-311++G(d,p) using scaling factors 0.960 in the high wavenumbers region and 0.988 in the low wavenumbers region [34]. (Conformer-1).

^b Obtained from the wave number calculated at B3LYP/6-311++G(d,p) using scaling factors 0.960 in the high wavenumbers region and 0.988 in the low wavenumbers region [34]. (Conformer-2)^cRelative absorption intensities normalized with highest peak absorption equal to 100.

^d Total energy distribution calculated B3LYP/6-311++G(d,p) level, PED less than 10% are not shown.

mostly located over imine group, (N-CH₃)₂ group and phenyl ring, the LUMO is mostly located over the pyridine ring, imine group. Consequently, the HOMO-LUMO transition implies an electron density transfer to pyridine group from the (N-CH₃)₂ group and phenyl ring.

The η value of **5**, **6**, and **7** was predicted at 1.656 eV, 1.681 eV, and 1.690 eV. The σ value of **5**, **6**, and **7** were determined at 0.302 eV, 0.297 eV and 0.296 eV. The global hardness (η) of the compounds was larger than the global softness (σ) of them (in Table 6). These results indicate that the compounds are *hard* ones. Whether a compound is *hard* or *soft* means that the compound has very different properties. For example, *hard* materials have a large energy gap while *soft* materials have a small energy gap. *Hard* compounds are not easily polarized, contrarily to *soft* ones. The biological reactivity of *soft* compounds is, therefore, higher than that of *hard* compounds [38–40].

3.7. Non linear optical properties

It is important to determine the nonlinear optical properties of materials. Theoretically, making (hyper) polarizability calculations might provide data for future studies of materials. The energy of a system in the weak and homogeneous electric field can be defined as:

$$E = E^0 - \mu_{\alpha}F_{\alpha} - \frac{1}{2}\alpha_{\alpha\beta}F_{\alpha}F_{\beta} - \frac{1}{6}\beta_{\alpha\beta\gamma}F_{\alpha}F_{\beta}F_{\gamma} - \dots \quad (5)$$

where E^0 is the total molecular energy in the absence of an electric field. F_{α} is the electric field component along the α direction. The μ_{α} , $\alpha_{\alpha\beta}$, and $\beta_{\alpha\beta\gamma}$ denote dipole moment, polarizability and the first order hyperpolarizability, respectively [13]. The dipole moment (μ), the mean polarizability ($\bar{\alpha}$), and the first order hyperpolarizability (β_0) are defined as:

$$\mu^2 = \mu_x^2 + \mu_y^2 + \mu_z^2 \quad (6)$$

Table 4
Experimental and predicted vibrational wavenumber for **7** at B3LYP/6-311++G(d,p).

FT-IR	Freq ^a	Freq ^b	I _{IR} ^c	TED ^d
513	520	517	2.512	$\Gamma_{\text{CCCH}}(21\%)+\Gamma_{\text{CCCC}}(11\%)+\Gamma_{\text{CNCC}}(10\%)+\Gamma_{\text{HCCN}}(10\%)+\beta_{\text{CNC}}(10\%)$
542	531	530	8.835	$\Gamma_{\text{CCCH}}(30\%)+\Gamma_{\text{CCNC}}(28\%)+\Gamma_{\text{CCCC}}(13\%)+\Gamma_{\text{HCCN}}(14\%)$
614	545	546	1.767	$\beta_{\text{CCH}}(23\%)+\beta_{\text{CCC}}(19\%)+\beta_{\text{CNC}}(13\%)+\beta_{\text{CCN}}(11\%)$
746	622	622	6.757	$\Gamma_{\text{CCCH}}(30\%)+\Gamma_{\text{CNCC}}(27\%)+\Gamma_{\text{HCCN}}(18\%)+\Gamma_{\text{CCCC}}(15\%)$
780	646	646	6.099	$\Gamma_{\text{CCCH}}(35\%)+\Gamma_{\text{HCCN}}(20\%)+\Gamma_{\text{CNCC}}(14\%)+\Gamma_{\text{CCCC}}(12\%)$
792	647	647	1.980	$\Gamma_{\text{CCCH}}(54\%)+\Gamma_{\text{HCCN}}(27\%)$
820	724	722	23.26	$\Gamma_{\text{CCCH}}(30\%)+\Gamma_{\text{HCCN}}(23\%)+\Gamma_{\text{CCCC}}(11\%)+\Gamma_{\text{CNCC}}(11\%)$
875	734	736	4.065	$\Gamma_{\text{CCCH}}(23\%)+\nu_{\text{CC}}(14\%)+\beta_{\text{CCH}}(14\%)+\beta_{\text{CNC}}(10\%)$
947	747	747	1.232	$\Gamma_{\text{CCCH}}(47\%)+\Gamma_{\text{HCCN}}(19\%)+\Gamma_{\text{CCCC}}(13\%)$
970	781	781	2.644	$\Gamma_{\text{CCCH}}(38\%)+\Gamma_{\text{HCCN}}(32\%)$
990	795	795	1.946	$\beta_{\text{CCC}}(20\%)+\beta_{\text{CCH}}(20\%)+\nu_{\text{CC}}(14\%)+\beta_{\text{CNC}}(13\%)+\nu_{\text{CN}}(10\%)$
1044	823	823	1.629	$\beta_{\text{CCH}}(38\%)+\nu_{\text{CC}}(28\%)$
1064	841	841	7.829	$\Gamma_{\text{HCCN}}(37\%)+\beta_{\text{HCCN}}(31\%)+\beta_{\text{HCH}}(10\%)+\nu_{\text{CN}}(10\%)$
1090	882	883	0.572	$\beta_{\text{CCH}}(48\%)+\nu_{\text{CC}}(17\%)$
1124	904	904	26.33	$\Gamma_{\text{HCCN}}(36\%)+\beta_{\text{HCCN}}(27\%)$
1147	936	937	0.859	$\beta_{\text{CCH}}(47\%)+\nu_{\text{CC}}(14\%)$
1168	950	949	2.000	$\beta_{\text{CCH}}(71\%)+\nu_{\text{CC}}(16\%)$
1228	951	952	12.85	$\Gamma_{\text{HCCN}}(20\%)+\nu_{\text{CC}}(17\%)+\beta_{\text{CCH}}(16\%)+\beta_{\text{HCCN}}(14\%)+\nu_{\text{CN}}(12\%)$
1278	967	966	0.632	$\beta_{\text{CCH}}(38\%)+\nu_{\text{CC}}(16\%)+\beta_{\text{HCCN}}(15\%)+\nu_{\text{CN}}(12\%)$
1302	982	982	1.320	$\beta_{\text{CCH}}(35\%)+\nu_{\text{CC}}(23\%)+\nu_{\text{CN}}(11\%)$
1365	996	996	88.38	$\Gamma_{\text{HCCN}}(20\%)+\beta_{\text{CCH}}(19\%)+\beta_{\text{HCCN}}(15\%)+\beta_{\text{HCH}}(12\%)+\nu_{\text{CN}}(11\%)$
1430	1002	1002	0.217	$\beta_{\text{HCH}}(28\%)+\beta_{\text{HCCN}}(27\%)+\beta_{\text{CCH}}(12\%)+\Gamma_{\text{HCCN}}(11\%)$
1466	1005	1005	9.754	$\beta_{\text{HCH}}(29\%)+\beta_{\text{HCCN}}(28\%)+\beta_{\text{CCH}}(16\%)+\Gamma_{\text{HCCN}}(11\%)$
1519	1049	1049	12.24	$\Gamma_{\text{HCCN}}(34\%)+\beta_{\text{HCH}}(31\%)+\beta_{\text{CCH}}(14\%)+\beta_{\text{HCCN}}(11\%)$
1571	1065	1065	3.346	$\beta_{\text{CCH}}(27\%)+\nu_{\text{CC}}(25\%)+\beta_{\text{CCC}}(12\%)+\beta_{\text{CNC}}(11\%)$
1590	1097	1097	7.771	$\beta_{\text{CCH}}(36\%)+\nu_{\text{CC}}(24\%)+\beta_{\text{CCC}}(11\%)+\nu_{\text{CN}}(11\%)$
1606	1116	1115	100	$\beta_{\text{CCH}}(36\%)+\nu_{\text{CC}}(24\%)+\beta_{\text{CCC}}(11\%)+\nu_{\text{CN}}(10\%)$
1619	1127	1128	37.89	$\beta_{\text{CCH}}(35\%)+\nu_{\text{CC}}(25\%)+\beta_{\text{CCC}}(10\%)$
2808	1135	1135	26.59	$\nu_{\text{CH}}(82\%)$
2890	1155	1155	47.08	$\nu_{\text{CH}}(78\%)$
2924	1175	1175	11.99	$\nu_{\text{CH}}(75\%)$
3008	1181	1181	15.38	$\nu_{\text{CH}}(75\%)$
3046	1225	1225	1.486	$\nu_{\text{CH}}(76\%)$

ν : Stretching, δ : Bending, τ : Torsion.

^a Obtained from the wave number calculated at B3LYP/6-311++G(d,p) using scaling factors 0.960 in the high wavenumbers region and 0.988 in the low wavenumbers region [34]. (Conformer-1).

^b Obtained from the wave number calculated at B3LYP/6-311++G(d,p) using scaling factors 0.960 in the high wavenumbers region and 0.988 in the low wavenumbers region [34]. (Conformer-2)^cRelative absorption intensities normalized with highest peak absorption equal to 100.

^d Total energy distribution calculated B3LYP/6-311++G(d,p) level, PED less than 10% are not shown.

Table 5
The experimental and calculated chemical shifts for ¹H and ¹³C nuclei.

Compound-5			Compound-6			Compound-7		
Atom	Theo.	Exp.	Atom	Theo.	Exp.	Atom	Theo.	Exp.
C ₂₇	156.7	152.1	C ₂₅	158.5	151.9	C ₂₃	163.0	155.4
C ₂₈	155.9		C ₂₄	156.8		C ₂₁	159.2	
C ₇	155.8		C ₄	155.3	151.1	C ₄	155.6	155.3
C ₂₁	154.9		C ₂₁	154.2	150.5	C ₂₈	155.4	150.1
C ₂₃	150.0	150.3	C ₆	145.4	149.9	C ₆	144.6	149.5
C ₅	144.8	143.7	C ₂₃	139.1	140.0	C ₂₇	141.0	139.4
C ₂	135.9	139.2	C ₂₆	137.3	134.3	C ₃	135.4	136.4
C ₂₆	129.3	122.8	C ₅	134.6	132.5	C ₂₄	128.2	124.2
C ₂₅	122.8	121.8	C ₂₇	128.2	123.7	C ₂₆	125.0	122.9
C ₆	120.3		C ₃	120.4	122.4	C ₅	120.8	121.3
C ₃	115.1	112.5	C ₇	115.3	112.7	C ₂	115.4	112.6
C ₄	114.8		C ₂	114.5		C ₇	114.5	
C ₁₂	40.47	40.5	C ₁₂	40.52	40.6	C ₁₆	40.51	40.5
C ₁₆	40.43		C ₁₆	40.43		C ₁₂	40.45	
H ₃₁	8.85	8.73	H ₂₉	8.87	9.00	H ₃₁	8.82	8.70
H ₃₂	8.81		H ₃₂	8.75		H ₂₂	8.82	
H ₂₂	8.70	8.52	H ₃₀	8.83	8.66	H ₂₉	8.59	8.21
H ₂₉	8.36	7.75	H ₂₂	8.71	8.57	H ₃₀	7.90	7.79
H ₃₀	7.50		H ₈	7.52	7.39	H ₈	7.66	7.42–7.37
H ₁	7.59	7.40–	H ₁₀	7.52		H ₁₀	7.55	7.28
H ₉	7.55	7.32	H ₃₁	7.50	7.32	H ₃₂	7.38	7.32
H ₈	6.83	6.82–	H ₉	6.79	6.78	H ₁	6.81	6.81–
H ₁₀	6.79	6.74	H ₁	6.77		H ₉	6.77	6.76
H ₁₉	3.37	3.05	H ₁₉	3.39	3.02	H ₁₃	3.39	3.03
H ₁₄	3.34		H ₁₄	3.35		H ₁₇	3.36	
H ₁₃	2.94		H ₁₃	2.90		H ₁₉	2.90	
H ₁₇	2.92		H ₁₇	2.86		H ₁₄	2.88	
H ₁₈	2.76		H ₁₅	2.77		H ₁₈	2.77	
H ₁₅	2.76		H ₁₈	2.76		H ₁₅	2.77	

Table 6
HOMO, LUMO, HOMO-LUMO gap and selected molecular properties of **5**, **6** and **7**.

		Energy (eV)	Energy gap (eV)	Ionization Potential (I) (eV)	Electron affinity (A) (eV)	Global Hardness (η) (eV)	Electronegativity (χ) (eV)	Chemical potential (μ) (eV)	Global Softness (σ) (eV) ⁻¹	Global electrophilicity (ω) (eV)
5	HOMO	-5.414	$\Delta E_{\text{HOMO-LUMO}}$	5.414	2.102	1.656	3.758	-3.758	0.302	4.265
	LUMO	-2.102								
	HOMO-1	-7.101	$\Delta E_{(H-1)-(L+1)}$	7.040	7.101	3.520	3.581	-3.581	0.142	1.822
	LUMO+1	-0.061								
6	HOMO	-5.309	$\Delta E_{\text{HOMO-LUMO}}$	3.362	5.309	1.946	3.628	-3.628	0.297	3.914
	LUMO	-1.946								
	HOMO-1	-7.027	$\Delta E_{(H-1)-(L+1)}$	6.122	7.027	3.061	3.966	-3.966	0.163	2.569
	LUMO+1	-0.905								
7	HOMO	-5.257	$\Delta E_{\text{HOMO-LUMO}}$	3.381	5.257	1.690	3.567	-3.567	0.296	3.763
	LUMO	-1.877								
	HOMO-1	-6.953	$\Delta E_{(H-1)-(L+1)}$	6.069	6.953	3.034	3.919	-3.919	0.165	2.530
	LUMO+1	-0.884								

$$I = -E_{\text{HOMO}}, A = -E_{\text{LUMO}}, \eta = \frac{(I-A)}{2}, \chi = \frac{(I+A)}{2}, \mu = \frac{-(I+A)}{2}, \sigma = \frac{1}{2\eta}, \omega = \frac{\mu^2}{2\eta}$$

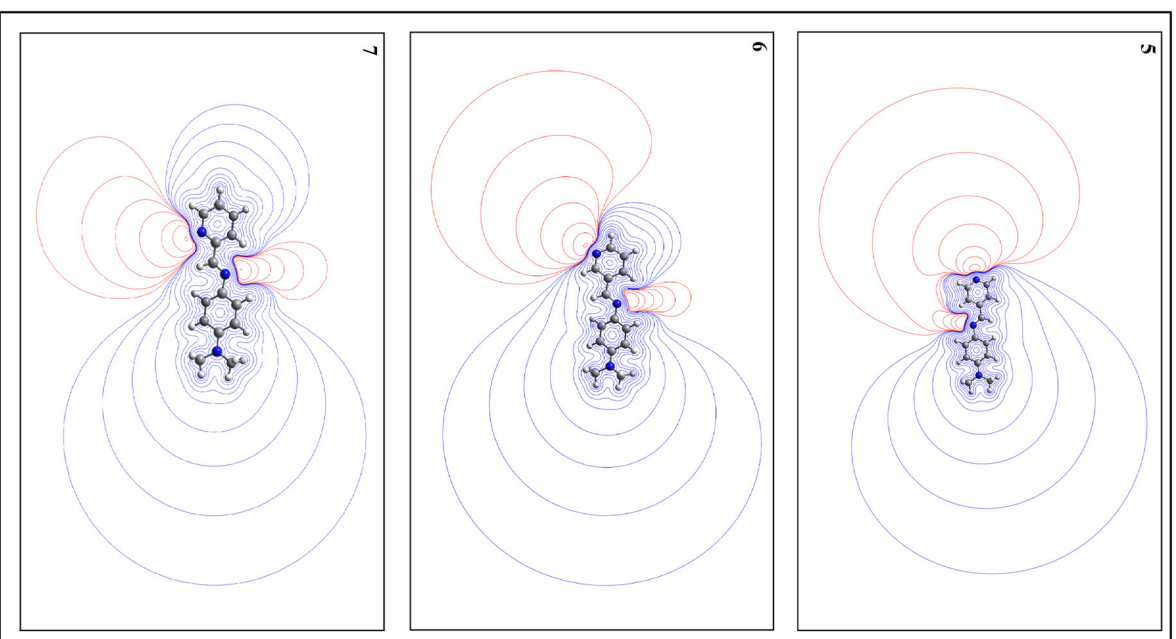


Fig. 4. Molecular electron potential contours of **5**, **6** and **7**.

Table 7

Theoretically calculated nonlinear optical properties of **5**, **6** and **7**.

	μ (Debye)	α ($\times 10^{-24}$ esu)	β_{tot} ($\times 10^{-30}$ esu)
Compound-5	6.337	34.953	89.838
Compound-6	4.432	34.689	78.648
Compound-7	2.440	34.933	85.514

$$\bar{\alpha} = (\alpha_{xx} + \alpha_{yy} + \alpha_{zz})/3 \quad (7)$$

$$\beta_0 = [(\beta_{xxx} + \beta_{xyy} + \beta_{xzz})^2 + (\beta_{yyx} + \beta_{xyx} + \beta_{yzz})^2 + (\beta_{zzx} + \beta_{xzz} + \beta_{yzz})^2]^{1/2} \quad (8)$$

As can be seen in Table 7, the predicted values of the dipol moment (μ) for **5**, **6**, and **7** were predicted at 6.337 D, 4.432 D, and 2.240 D by B3LYP/6-311++G(d,p). The mean polarizability values were determined as 34.95×10^{-24} esu, 34.68×10^{-24} esu, and 34.93×10^{-24} esu for **5**, **6**, and **7** respectively. Hyperpolarizability

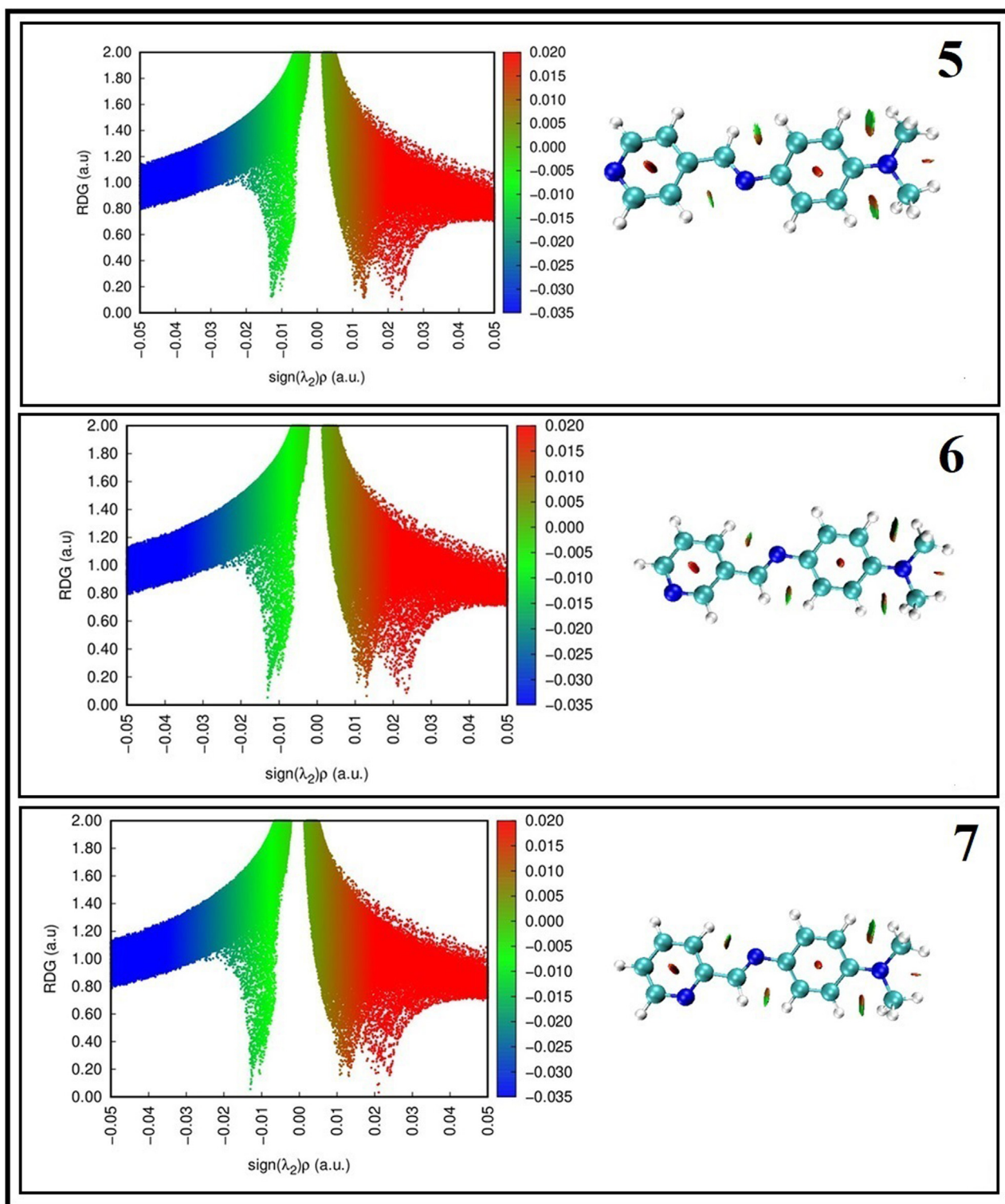


Fig. 5. RDG scatter plots (left) and corresponding non-covalent interaction (NCI) plots (right) of **5**, **6** and **7**. The isosurfaces are colored (right) with respect to the values of $\text{sign}(\lambda_2)\rho$ (a.u.).

values of **5**, **6**, and **7** were found 89.83×10^{-30} esu, 78.64×10^{-30} esu, and 85.51×10^{-30} esu, respectively.

In the literature, urea is widely used to compare dipole moment and hyperpolarizability values. Therefore, we compared the dipole moment and hyperpolarizability values of **5**, **6**, and **7** with urea. When compared to the urea, which has a dipole moment of 1.373 D, the dipole moment of **5**, **6**, and **7** were found to be 4.61, 3.22, and

1.77 times greater. Compared with urea's first hyperpolarizability value (0.3728×10^{-30} esu for urea), the hyperpolarizability value of the **5**, **6**, and **7** were determined to be 240, 210, and 229 times greater than that of urea. **5**, **6**, and **7** had a very high first hyperpolarizability. The high hyperpolarizability value and non-zero value of dipole moment indicated that **5**, **6**, and **7** might be a good candidate of NLO material (Table 3).

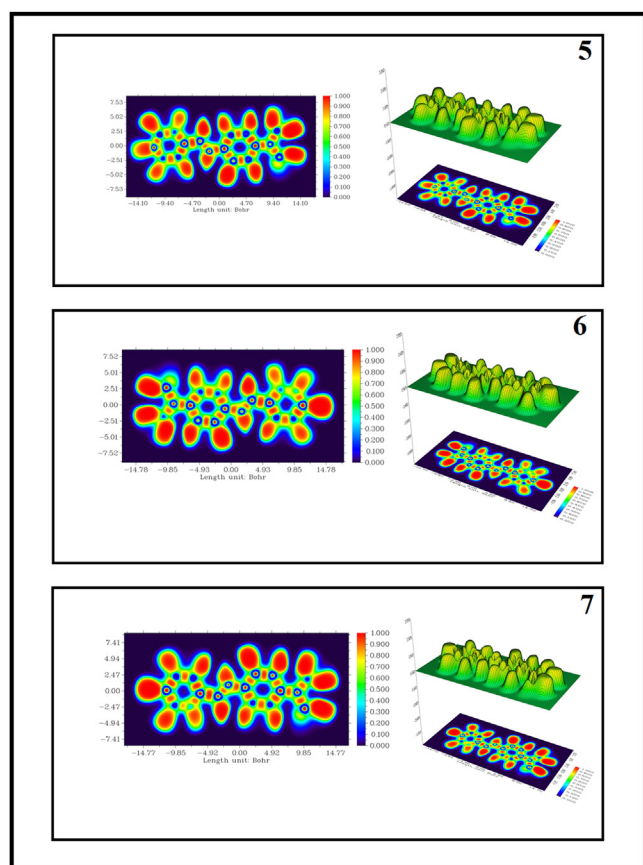


Fig. 6. Color filled map of Electron localization function (ELF) of **5**, **6** and, **7**.

3.8. Molecular electrostatic potential maps

A 3D plot of the molecular electrostatic potential (MEP) of **5**, **6**, and, **7** were given in Fig. 4. The reactive regions of the compounds could be easily identified via the MEP diagram. The red regions showed electron-rich regions, and the blue regions showed electron-poor regions. The region around the nitrogen atom of the pyridine ring and imine group was found to be electron-rich. [41,42].

3.9. Reduced density gradient

The Reduced Density Gradient (RDG) gives an analysis that visualizes the regions where intra and inter non-covalent interactions occur in a compound. The Reduced Density Gradient (RDG) analysis were completed using Multiwfn program. Gradient iso-

surfaces and scatter plots of **5**, **6**, and, **7** were shown in Fig. 5. The RDG scatter plot was created between RDG versus $\text{sign}(\lambda_2)\rho$. The $\text{sign}(\lambda_2)\rho$ was the second Eigenvalue of electron density. $\text{Sign}(\lambda_2)\rho$ value and sign were used to explain the nature of interactions. If $\text{sign}(\lambda_2)\rho$ was greater than zero, repulsive interaction would occur, and if $\text{sign}(\lambda_2)\rho$ was less than zero, attractive interaction would occur, and if $\text{sign}(\lambda_2)\rho$ was zero, weak Van der Waals interaction would occur. The function of $\lambda_2(r)$ in the RDG scattering spectrum divided into three colors as red, green, and blue was between -0.035 and 0.020 a.u. The color-coding scheme for 3D spatial visualization of RDG surface indicated blue for attractive, red for repulsive, and green for intermediate interactions [43,44].

In the RDG isosurfaces, the red spike showed the steric repulsion in the centers of phenyl and pyridine rings. The RDG scatter plot shows red contour between 0.02 and 0.05 au, clarifies higher repulsive change contribution. The red-green mixed spikes were observed near the N-CH₃ and imine groups. The RDG scatter plot shows the red-green mixed spikes between 0.00 and 0.015 au The RDG graph results confirmed the interacting regions in the molecular structure of **5**, **6**, and, **7**.

3.10. Electron localization function

The Electron Localization Function (ELF) analysis were completed using Multiwfn program [45]. The possibility of finding an electron with the same spin in the neighborhood concerning an electron located at a given point (reference electron) could be measured using ELF. For **5**, **6**, and, **7**, two-dimensional plots of the ELF are shown in Fig. 6. In the scale, red color (0.8 – 1.0) represented high ELF values; the low ELF regions were shown in blue, and the intermediate region was represented in green. The red color which surrounded the hydrogen atoms with maximum value indicated the presence of bonding and nonbonding electrons. The blue color cloud around the carbon and nitrogen atoms indicated a low electron localization values as represented in Fig. 6. For the **5**, **6**, and, **7**, the maximum Pauli repulsion was found around the Hydrogen atoms as indicated in red, and the minimum Pauli repulsion is for Carbon and Nitrogen atoms as indicated by blue region [46].

3.11. Antimicrobial evaluation of the synthesized compounds

The synthesized compounds were evaluated for their antimicrobial screening against selected bacteria such as *L. monocytogenes* ATCC 7644, *S. aureus* ATCC 25923, *B. subtilis* ATCC 6633, *E. faecalis* ATCC 29212, *K. pneumonia* ATCC 21541, *P. aeruginosa* ATCC 27853, *S. dysenteriae* ATCC 11835, *S. typhimurium* ATCC 14028, *E. coli* ATCC 25922 and yeast such as *C. albicans* ATCC 10231 by both microdilution and disk diffusion methods. Results of antimicrobial activity of the compounds all with Minimal Inhibitory Concentration (MIC) and inhibition zone diameter (mm) were shown in Table 8. Based

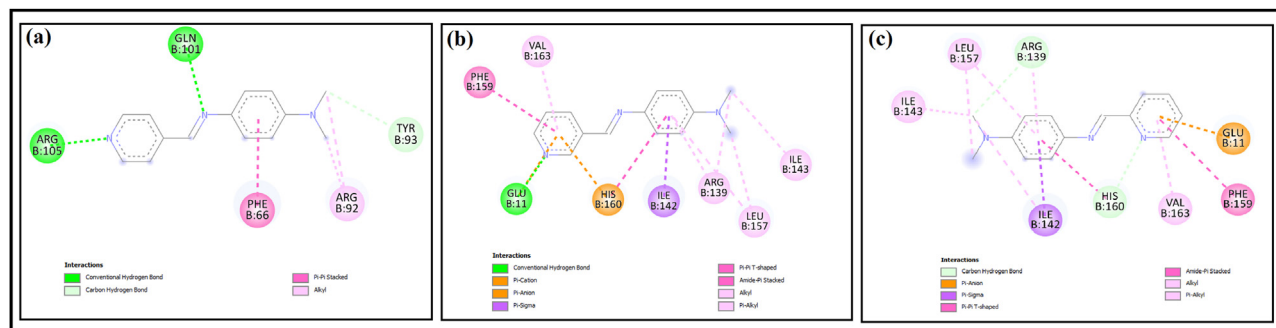


Fig. 7. The interacting mode with 4QGG in 2D representations of compound **5** (a), **6** (b), **7** (c).

Table 8
Antimicrobial and antifungal evaluation of **5**, **6** and **7**. MIC ($\mu\text{g}/\text{mL}$) values and the inhibition zone diameter (mm).

Microorganisms	MIC ($\mu\text{g}/\text{mL}$)			Diameter of inhibition zone (mm)				
	Compounds (1000 $\mu\text{g}/\text{ml}$)			Compounds (1000 $\mu\text{g}/\text{ml}$)				
	5	6	7	5	6	7	AMP (10 μg)	Cycloheximide
<i>L. monocytogenes</i> ATCC 7644	–	–	–	–	–	–	10	–
<i>S. aureus</i> ATCC 25923	–	1.95	1.95	–	20	20	18	–
<i>B. subtilis</i> ATCC 6633	–	62.5	62.5	–	12	12	24	–
<i>E. faecalis</i> ATCC 29212	–	–	250	–	–	10	–	–
<i>K. pneumoniae</i> ATCC 21541	–	–	250	–	–	10	–	–
<i>P. aeruginosa</i> ATCC 27853	250	–	7.81	10	–	15	18	–
<i>S. dysenteriae</i> ATCC 11835	–	250	250	–	10	10	20	–
<i>S.typhimurium</i> ATCC 14028	–	–	–	–	–	–	18	–
<i>E. coli</i> ATCC 25922	–	–	7.81	–	–	15	–	–
<i>C. albicans</i> ATCC 10231	250	7.81	62.5	10	15	12	–	18

MIC >250.

Amp: Ampicillin.

Table 9
Docking parameters of title compounds docked with the 4QGG protein target.

Compound	Bonded residues	No of hydrogen bonds	Bonded distance (Å)	Binding energy (kcal/mol)	Inhibition Constant K_i (μM)	Reference RMSD(Å)
5	GLN 101	3	2.03	–6.44	19.10	34.81
	ARG 105		2.48			
	ARG 105		1.70			
6	GLU 11	2	1.94	–5.89	48.49	45.62
	TYR 100		2.47			
7	GLU 11	1	2.73	–5.47	97.20	46.52

on the findings of the present study, the MIC values of the compounds ranged from 1.95 to 250 $\mu\text{g}/\text{ml}$ for antimicrobial activity against *S. aureus*, *B. subtilis*, *E. faecalis*, *K. pneumoniae*, *P. aeruginosa*, and *S. dysenteriae*. Compound **7** was found to be the most active against bacteria and yeast while compound **5** was found to be moderately active. Compounds **6** (against *S. aureus* and *C. albicans*) and **7** were found to have a very high minimum inhibitory concentration ranging between 1.95 and 7.81 g/mL (against *P. aeruginosa* and *E. coli*). Compounds (**6** and **7**) showed zone of inhibition values in the range of 10–20 mm against other bacteria except for *L. monocytogenes* and *S. typhimurium*. *C. albicans* showed good activity against all compounds (**5**, **6**, and **7**) with a MIC value of 1.95–250 $\mu\text{g}/\text{ml}$. In addition, all compounds (**5**, **6**, and **7**) tested against *C. albicans* showed high levels of antifungal activity (Table 8).

3.12. Molecular docking

The molecular docking of the chemical compounds-proteins binding site was performed using Autodock 2.2.6 software [47] The docked complexes were visualized using Chimera [27] and Discover studio software [48] The target proteins' crystal structures were taken from the RCSB database (www.pdb.org).

As shown in Table 9, the docking parameters calculated inhibition constant, binding energy, and hydrogen bond distance all play a role in determining the type of the molecule. The binding interactions of the compound with protein are depicted in Fig. 7. From the docking results in Table 9 and Fig. 7. The compounds and 4QGG (receptor) with a binding energy values are –6.44, –5.89, –5.47 kcal/mol, respectively. These results show that the protein targets under consideration, compound 5, show the best pharmacological activity against 4QGG with lower binding energies and K_i values. All proteins, the hydrogen bonded amino acids bond length is with the <3 Å which indicate they are all strong hydrogen bonding interaction. As can be seen from the results in Table 9, the compound interacted with the amino acids of the receptor through hydrogen bonding. In Fig. 7, the pyridine ring of the compound **5** interacted with residues of the protein by hydrogen bonding

with ARG'105 and GLN'101. Similarly, H-bond interactions involving residues GLU'11, TYR'100 with compounds **6** and **7**.

4. Conclusion

The present study reported that microwave-assisted preparation of a series of Schiff bases without the use of a solvent was possible. The structures of synthesized compounds were confirmed by FT-IR and NMR spectroscopy. Two conformers of the **5**, two conformers of the **6**, and four conformers of the **7** were determined using the PES scan result. The most stable conformers of the compounds were determined and then re-optimized by using 6-311++G(d,p) basis set for future calculations. There appeared to be a perfect agreement between the experimental FT-IR, ^1H , and ^{13}C NMR data, and the theoretical ones of the most stable isomer. The compounds **5**, **6**, and **7** had a very high first hyperpolarizability. The high hyperpolarizability value and non-zero value of dipole moment indicated that **5**, **6**, and **7** might be a good candidate of NLO material. Investigation of antimicrobial screening data revealed that the compounds (**6** and **7**) showed maximum zone of inhibition against nearly all bacteria (except *L. monocytogenes* ATCC 7644, *S.typhimurium* ATCC 14028) and yeast. Compounds (**6** and **7**) showed a maximum zone of inhibition (20 mm) specifically against *S. aureus* ATCC 25923. The antibacterial activity of the molecules synthesized were found to be $5 < 6 < 7$. This is thought to be owing to the compounds' structural stability. The synthesized compounds exhibited significant antimicrobial activity. **5** were determined to dock with the energetic spot of ARG'105 and GLN'101. Similarly, **6** and **7** were determined to dock with the energetic spot of GLU'11, TYR'100.

Captions of supplementary material

- Fig. S1 Experimental FT-IR spectra of **5**, **6** and **7**
- Fig. S2 ^1H and ^{13}C NMR spectra of compound-**5**
- Fig. S3 ^1H and ^{13}C NMR spectra of compound-**6**
- Fig. S4 ^1H and ^{13}C NMR spectra of compound-**7**

Fig. S5 Torsional barriers results of **5**, **6** and, **7**.
Table S1 Optimized geometric parameters of **5**, **6** and, **7**

Declaration of Competing Interest

The authors declare that they have no known competing financial interests or personal relationships that could have appeared to influence the work reported in this paper.

CRediT authorship contribution statement

M. Ayaz: Investigation, Writing – review & editing. **Ö. Gündoğdu:** Methodology, Resources, Writing – review & editing. **S. Aytac:** Methodology, Writing – original draft, Writing – review & editing. **B. Erdem:** Investigation, Resources, Writing – original draft. **H. Çiftçi:** Writing – review & editing, Resources. **Y. Erdogdu:** Investigation, Writing – original draft, Writing – review & editing, Supervision.

Data availability

Data will be made available on request.

Acknowledgment

This work is based on Melike AYAZ PhD thesis. We thanks to Dr. M. Tahir GÜLLÜOĞLU for Gaussian 16 software and Dr. Sibel ÇELİK for Molecular Docking calculation. The Quantum Chemical calculations reported in this paper were fully performed at Harran University High Performance Computing Center (Harran HPC resources).

Supplementary materials

Supplementary material associated with this article can be found, in the online version, at doi:[10.1016/j.molstruc.2022.133791](https://doi.org/10.1016/j.molstruc.2022.133791).

References

- L. Xia, Y. Zhang, J. Zhang, S. Lin, K. Zhang, H. Tian, Y. Dong, H. Xu, Identification of novel thiazolo[5,4-b]pyridine derivatives as potent phosphoinositide 3-kinase inhibitors, *Molecules* 25 (2020) 4630, doi:[10.3390/molecules25204630](https://doi.org/10.3390/molecules25204630).
- A.Y. Guan, C.L. Liu, X.F. Sun, Y. Xie, M.A. Wang, Discovery of pyridine-based agrochemicals by using intermediate derivatization methods, *Bioorg. Med. Chem.* 24 (2016) 342–353, doi:[10.1016/j.bmc.2015.09.031](https://doi.org/10.1016/j.bmc.2015.09.031) 0968–0896.
- L. Wei, W. Tan, J. Zhang, Y. Mi, F. Dong, Q. Li, Z. Guo, Synthesis, characterization, and antifungal activity of Schiff bases of inulin bearing pyridine ring, *Polymers* 11 (2019) 371 (Basel), doi:[10.3390/polym11020371](https://doi.org/10.3390/polym11020371).
- C.H. Kline, J. Turkevich, Catalytic synthesis of pyridine, *J. Am. Chem. Soc.* 66 (1944) 1710–1714, doi:[10.1021/ja01238a031](https://doi.org/10.1021/ja01238a031).
- K. Chapaneri, *One-Pot Methodology for the Synthesis of Polysubstituted Pyridines and Terpyridines*, Cardiff University Thesis of Doctor of Philosophy, U.K., 2008.
- A.K. Alnomsy, *Synthesis and Properties of Pyridine Containing Drugs and heterocycles*, School of Life Sciences University of Sussex, 2016 Doctor of Philosophy Thesis.
- M. Baumann, I.R. Baxendale, An overview of the synthetic routes to the best selling drugs containing 6-membered heterocycles, *Beilstein J. Org. Chem.* 9 (2013) 2265–2319, doi:[10.3762/bjoc.9.265](https://doi.org/10.3762/bjoc.9.265).
- P.P. Parashar, *Introductory Chapter, Pyridine*, 2018 ISBN: 978-1-78923-422-0, doi:[10.5772/intechopen.77969](https://doi.org/10.5772/intechopen.77969).
- E. Khan, Pyridine derivatives as biologically active precursors; organics and selected coordination complexes, *ChemistrySelect* 6 (13) (2021) 3041–3064, doi:[10.1002/slct.202100332](https://doi.org/10.1002/slct.202100332).
- J.J. Vora, S.B. Vasava, K.C. Parmar, S.K. Chauhan, S.S. Sharma, Synthesis, spectral and microbial studies of some novel Schiff base derivatives of 4-methylpyridin-2-amine, *Eur. J. Chem.* 6 (2009) 1205–1210, doi:[10.1155/2009/247209](https://doi.org/10.1155/2009/247209).
- W. Behja, M. Jemal, Anti-HIV drug discovery, development and synthesis of delavirdine: review article, *Int. Res. J. Pure Appl. Chem.* 20 (2019) 1–16, doi:[10.9734/irjpac/2019/v20i330137](https://doi.org/10.9734/irjpac/2019/v20i330137).
- S. Shami, S. Murtaza, M.F. Nazar, Synthesis of Schiff bases of pyridine-4-carbaldehyde and their antioxidant and DNA binding studies, *J. Chem. Soc. Pak.* 38 (2016) 494–503 <https://www.researchgate.net/publication/307588263>.
- K.M. Khan, W. Jamil, M. Ambreen, M. Taha, S. Perveen, A. Guillermo, G.A. Morales, An expeditious synthetic approach towards the synthesis of Bis-Schiff bases (aldazines) using ultrasound, *Ultrason. Sonochem.* 21 (2011) 1200–1205, doi:[10.1016/j.ultrsonch.2013.12.011](https://doi.org/10.1016/j.ultrsonch.2013.12.011).
- S.K. Sridhar, M. Saravanan, A. Ramesh, Synthesis and antibacterial screening of hydrazones, Schiff and Mannich bases of isatin derivatives, *Eur. J. Med. Chem.* 36 (2001) 615–625, doi:[10.1016/S0223-5234\(01\)01255-7](https://doi.org/10.1016/S0223-5234(01)01255-7).
- A.H. Shntaif, Z.M. Rashid, The synthesis of Schiff bases under microwave irradiation, *Rev. J. Chem. Pharm. Sci.* 9 (2016) 1066–1068 ISSN: 0974-2115 www.jchps.com.
- R.W. Layer, The chemistry of imines, *Chem. Rev.* 63 (1963) 489–510, doi:[10.1021/cr60225a003](https://doi.org/10.1021/cr60225a003).
- C.M.D. Silva, D.L.D. Silva, L.V. Modolo, B.B. Alves, M.A.D. Resende, C.V.B. Martins, A.D. Fatima, Schiff bases: a short review of their antimicrobial activities, *J. Adv. Res.* 2 (2011) 1–8, doi:[10.1016/j.jare.2010.05.004](https://doi.org/10.1016/j.jare.2010.05.004).
- D. Becerra, J. Portilla, J. Cobo, J.C. Castillo, M.A. Macías, The effect of molecular planarity and resonant effects on supramolecular structures of N-(5-pyrazolyl)imines by X-ray crystallographic analysis, *J. Mol. Struct.* 1252 (2022) 132098, doi:[10.1016/j.molstruc.2021.132098](https://doi.org/10.1016/j.molstruc.2021.132098).
- F. Kamil, K.A. Hubeatir, M. Shamel, A.A. Al-Amiry, Microwave-assisted solvent-free synthesis of new polyimine, *Cogent Chem.* (1) (2015) 1075853 [1080/23312009.2015.1075853](https://doi.org/10.1080/23312009.2015.1075853).
- S. Handayani, C. Budimarwanti, W. Haryadi, Microwave-assisted organic reactions: eco-friendly synthesis of dibenzylidenecyclohexanone derivatives via crossed aldol condensation indones, *J. Chem.* 17 (2) (2017) 336–341.
- G. Hilt, J. Janikowski, M. Schwarzer, O. Burghaus, D. Sakow, M. Bröring, M. Drüscher, B. Huber, B. Roling, K. Harms, Studies of electronic effects of modified pyridine-imine ligands utilized in cobalt-catalyzed meta-selective Diels-Alder reactions, *J. Organomet. Chem.* 749 (2014) 219–223, doi:[10.1016/j.jorganchem.2013.09.020](https://doi.org/10.1016/j.jorganchem.2013.09.020).
- S. Aytac, in: Schiff Bazı Bileşiklerinin Çevreci Bir Yöntemle Yeniden Sentezi, 11. İğdır Üniversitesi Fen Bilimleri Enstitüsü Dergisi, 2021, pp. 2979–2991, doi:[10.21597/jist.976184](https://doi.org/10.21597/jist.976184).
- M.J. Frisch, et al., *Gaussian 16, Revision B.01*, Gaussian, Inc., Wallingford CT, 2016.
- A.D. Becke, Density-functional exchange-energy approximation with correct asymptotic behavior, *Phys. Rev. A* 38 (1988) 3098–3100, doi:[10.1103/PhysRevA.38.3098](https://doi.org/10.1103/PhysRevA.38.3098).
- A.D. Becke, Density-functional thermochemistry. III. The role of exact exchange, *J. Chem. Phys.* 98 (1993) 5648–5652 3, doi:[10.1063/1.46491](https://doi.org/10.1063/1.46491).
- C. Lee, W. Yang, R.G. Parr, Development of the Colle-Salvetti correlation-energy formula into a functional of the electron density, *Phys. Rev. B* 37 (1988) 785–789, doi:[10.1103/PhysRevB.37.785](https://doi.org/10.1103/PhysRevB.37.785).
- Y. Erdoğan, M.T. Güllüoğlu, S. Yurdakul, Ö. Dereli, DFT simulations, FT-IR, FT-Raman, and FT-NMR spectra of 4-(4-chlorophenyl)-1H-imidazole molecules, *Opt. Spectrosc.* 113 (2012) 23–32, doi:[10.1134/S0030400X12070089](https://doi.org/10.1134/S0030400X12070089).
- S. Saglam, A. Disli, Y. Erdogdu, M.K. Marchewka, N. Kanagathara, B. Bay, Synthesis, characterization and theoretical studies of 5-(benzylthio)-1-cylopentyl-1H-tetrazole, *Spectrochim. Acta Part A* 135 (2015) 1011–1018, doi:[10.1016/j.saa.2014.07.071](https://doi.org/10.1016/j.saa.2014.07.071).
- Y. Erdogdu, Ö. Dereli, D. Sajan, L. Joseph, O. Ünsalan, M.T. Güllüoğlu, Vibrational (FT-IR and FT-Raman) Spectral Investigations of 7-Amino flavone with density functional theoretical simulations, *Mol. Simul.* 38 (2012) 315–325, doi:[10.1080/08927022.2011.632416](https://doi.org/10.1080/08927022.2011.632416).
- Y. Erdogdu, T.R. Sertbakan, M.T. Gulluoglu, S. Yurdakul, A. Guvenir, FT-IR and Raman spectroscopy and computation of 5-methylfurfural, *J. Appl. Spectrosc.* 85 (2018) 517–525, doi:[10.1007/s10812-018-0682-9](https://doi.org/10.1007/s10812-018-0682-9).
- Clinical and Laboratory Standards Institute (CLSI). *Performance Standards for Antimicrobial Susceptibility Testing*, 30th ed., Clinical and Laboratory Standards Institute, Wayne, Pennsylvania USA, 2020.
- M. Hamana, B. Umezawa, S. Nakasima, Studies on tertiary amine oxides. XIII. Reactions of N-(p-dimethylaminophenyl)nitrones having pyridine N-oxide, quinoline or its N-oxide as α -substituent, *Chem. Pharm. Bull.* 10 (1962) 961–968, doi:[10.1248/cpb.10.961](https://doi.org/10.1248/cpb.10.961).
- A. Borba, M. Albrecht, A.G. Zavaglia, L. Lapinski, M.J. Nowak, M.A. Suhmb, R. Fausto, Dimer formation in nicotinamide and picolinamide in the gas and condensed phases probed by infrared spectroscopy, *Phys. Chem. Chem. Phys.* 10 (2008) 7010–7021, doi:[10.1039/B810002K.11](https://doi.org/10.1039/B810002K.11).
- M. Yilmaz, B. Aydin, O. Dogan, O. Dereli, Molecular structure and spectral investigations of 3,5-Di-tert-butyl-o-benzoquinone, *J. Mol. Struct.* 1128 (2017) 345–354, doi:[10.1016/j.molstruc.2016.08.067](https://doi.org/10.1016/j.molstruc.2016.08.067).
- E.K. Sarıkaya, S. Bahçeli, D. Varkal, O. Dereli, FT-IR, micro-Raman and UV-vis spectroscopic and quantum chemical calculation studies on the 6-chloro-4-hydroxy-3-phenyl pyridazine compound, *J. Mol. Struct.* 1141 (2017) 44–52, doi:[10.1016/j.molstruc.2017.03.088](https://doi.org/10.1016/j.molstruc.2017.03.088).
- Y. Erdogdu, Ş. Yurdakul, S. Badoglu, M.T. Güllüoğlu, Electronic [UV-visible] and vibrational [FT-IR] investigation and NMR spectroscopic analysis of some halogen substituted chromone (6-fluorochromone, 6-chlorochromone, 6-bromochromone), *J. Mol. Struct.* 1184 (2019) 364–374, doi:[10.1016/j.molstruc.2019.02.016](https://doi.org/10.1016/j.molstruc.2019.02.016).
- Y. Erdogdu, S. Saglam, M.T. Gulluoglu, An investigations on the molecular structure, FT-IR, FT-Raman and NMR spectra of 1-(p-tolylsulfonyl) pyrrole by theoretical and experimental approach, *Spectrochim. Acta Part A* 146 (2015) 88–96, doi:[10.1016/j.saa.2015.03.031](https://doi.org/10.1016/j.saa.2015.03.031).
- S. Celik, S. Yurdakul, B. Erdem, Synthesis, spectroscopic characterization (FT-IR, PL), DFT calculations and antibacterial activity of silver(I) nitrate complex with nicotinaldehyde, *Inorg. Chem. Commun.* 131 (2021) 108760, doi:[10.1016/j.inoche.2021.108760](https://doi.org/10.1016/j.inoche.2021.108760).
- S. Celik, M. Alp, S. Yurdakul, A combined experimental and theoretical study

- on vibrational spectra of 3-pyridyl methyl ketone, *Spectrosc. Lett.* 53 (2020) 234–248, doi:[10.1080/00387010.2020.1734840](https://doi.org/10.1080/00387010.2020.1734840).
- [40] S. Celik, S. Yurdakul, Investigations on spectroscopic characterizations, molecular docking, NBO, drug-Likeness, and ADME properties of 4H-1,2,4-triazol-4-amine by combined computational approach, *Eur. J. Chem.* 12 (2021) 401–411, doi:[10.5155/eurjchem.12.4.401-411.2165](https://doi.org/10.5155/eurjchem.12.4.401-411.2165).
- [41] Ö. Dereli, Y. Erdogdu, M.T. Gulluoglu, E. Türkkan, A. Özmen, N. Sundaraganesan, Vibrational spectral and quantum chemical investigations of tert-butylhydroquinone, *J. Mol. Struct.* 1012 (2012) 168–176, doi:[10.1016/j.molstruc.2012.01.003](https://doi.org/10.1016/j.molstruc.2012.01.003).
- [42] L. Joseph, D. Sajan, R. Reshmy, B.S.A. Sasi, K.K.T Y.Erdogdu, Vibrational spectra, structural conformations, scaled quantum chemical calculations and NBO analysis of 3-acetyl-7-methoxycoumarin, *Spectrochim. Acta Part A* 99 (2012) 234–247, doi:[10.1016/j.saa.2012.07.084](https://doi.org/10.1016/j.saa.2012.07.084).
- [43] J. Priscilla, D.A. Dhas, I.H. Joe, S. Balachandran, Spectroscopic, quantum chemical, hydrogen bonding, re duce d density gradient analysis and anti-inflammatory activity study on piper amide alkaloid piperine and wisanine, *J. Mol. Struct.* 1225 (2021) 129146, doi:[10.1016/j.molstruc.2020.129146](https://doi.org/10.1016/j.molstruc.2020.129146).
- [44] X.D.D. Dexlin, J.D.D. Tarika, S.M. Kumar, A. Mariappan, T.J. Beaula, Synthesis and DFT computations on structural, electronic and vibrational spectra, RDG analysis and molecular docking of novel anti COVID-19 molecule 3, 5 dimethyl pyrazolium 3, 5 dichloro salicylate, *J. Mol. Struct.* 1246 (2021) 131165, doi:[10.1016/j.molstruc.2021.131165](https://doi.org/10.1016/j.molstruc.2021.131165).
- [45] X.D.D. Dexlin, J.D.D. Tarika, S.M. Kumar, A. Mariappan, T.J. Beaula, Synthesis and DFT computations on structural, electronic and vibrational spectra, RDG analysis and molecular docking of novel anti COVID-19 molecule 3, 5 dimethyl pyrazolium 3, 5 dichloro salicylate, *J. Mol. Struct.* 1246 (2021) 131165, doi:[10.1016/j.molstruc.2021.131165](https://doi.org/10.1016/j.molstruc.2021.131165).
- [46] G.M. Morris, D.S. Goodwill, R.S. Halliday, R. Huey, W. Hart, R.K. Belew, A.J. Olson, Automated docking using a Lamarckian genetic algorithm and an empirical binding free energy function, *J. Comput. Chem.* 19 (1998) 1639–1662 doi:[10.1002/\(SICI\)1096-987X\(19981115\)19:14<1639::AID-JCC10>3.0.CO;2-B](https://doi.org/10.1002/(SICI)1096-987X(19981115)19:14<1639::AID-JCC10>3.0.CO;2-B).
- [47] D.S. Biovia, Dassault Systèmes; San Diego: 2016. Discovery Studio Visualizer, v17.2.0.16349.
- [48] T. Lu, F. Chen, Multiwfn: A multifunctional wavefunction analyzer, *J. Comput. Chem.* (2011) 580–592, doi:[10.1002/jcc.22885](https://doi.org/10.1002/jcc.22885).